applied sciences

MDPI

Article

Tunable Dual Broadband Terahertz Metamaterial Absorber Based on Vanadium Dioxide

Xiao-Fei Jiao [1,2,3], Zi-Heng Zhang [1,2,3], Tong Li [4], Yun Xu [1,2,3] and Guo-Feng Song [1,2,3,*]

1 Institute of Semiconductors, Chinese Academy of Sciences, Beijing 100083, China; xfjiao@semi.ac.cn (X.-F.J.); zhzhang92@semi.ac.cn (Z.-H.Z.); xuyun@semi.ac.cn (Y.X.)
2 College of Materials Science and Opto-Electronic Technology, University of Chinese Academy of Sciences, Beijing 100049, China
3 Beijing Key Laboratory of Inorganic Stretchable and Flexible Information Technology, Beijing 100083, China
4 School of Physics and Electronic Sciences, Changsha University of Science and Technology, Changsha 410004, China; lt@csust.edu.cn
* Correspondence: sgf@semi.ac.cn

Received: 15 August 2020; Accepted: 13 October 2020; Published: 17 October 2020

Abstract: With the rapid development of terahertz technology, tunable high-efficiency broadband functional devices have become a research trend. In this research, a dynamically tunable dual broadband terahertz absorber based on the metamaterial structure of vanadium dioxide (VO_2) is proposed and analyzed. The metamaterial is composed of patterned VO_2 on the top layer, gold on the bottom layer and silicon dioxide (SiO_2) as the middle dielectric layer. Simulation results show that two bandwidths of 90% absorption reach as wide as 2.32 THz from 1.87 to 4.19 THz and 2.03 THz from 8.70 to 10.73 THz under normal incidence. By changing the conductivity of VO_2, the absorptance dynamically tuned from 2% to 94%. Moreover, it is verified that absorptance is insensitive to the polarization angle. The physical origin of this absorber is revealed through interference theory and matching impedance theory. We further investigate the physical mechanism of dual broadband absorption through electric field analysis. This design has potential applications in imaging, modulation and stealth technology.

Keywords: terahertz; metamaterial; vanadium dioxide; perfect absorber

1. Introduction

Terahertz (THz) waves generally refer to electromagnetic waves with a frequency ranging from 0.1 to 10.0 THz. They have a wide range of applications in the fields of wireless communication, sensors and imaging [1–3]. Because of their bright future, they have aroused great interest in the past few decades. With the rapid development of THz technology, the performance requirements of related functional devices are gradually increasing. Traditional natural materials have inherent shortcomings such as performance limitations, bulky and difficulty of integration, which can no longer meet the current needs for optic applications. Metamaterials (MM) composed of periodic subwavelength antenna arrays can solve the above problems. Because MM have the advantages of high efficiency, tunability and easy integration, various functional devices based on MM have been proposed, such as optical filters, absorbers and polarization converters [4–9]. Among various devices, the metamaterial perfect absorber (MPA) has received widespread attention due to its significant role in imaging, stealth technology and sensing applications [10–12]. The first MPA working in the microwave band was proposed by Landy et al. in 2008 [13]. A metal–insulator–metal (MIM) configuration is used to demonstrate MPAs. The basic unit structure of MPAs usually consists of three functional layers: a patterned metal layer on the top layer, a metal layer on the bottom layer and a dielectric layer in the middle. Under the guidance of this design, many types of MPAs have been reported, and the research

on them is not limited to the microwave frequency range but gradually extends to all spectra related to technology, including THz, infrared, visible light and ultraviolet ranges [14–20]. So far, various MM have realized absorbers that work at THz frequencies. However, once the structure of the traditional MM absorber is determined, the electromagnetic response cannot be adjusted, and it has a fixed peak frequency and absorptance, which limits their practical application.

MPAs based on semiconductors, graphene and liquid crystals have been reported to realize the dynamic tunable characteristics [21–23]. Vanadium dioxide (VO_2), as a phase change material, varies greatly during the phase transition from insulator to metal by changing the temperature [24]. This is caused by the transformation of the structure from the insulating monoclinic phase to the metallic tetragonal phase around 68 °C. Therefore, combining MM with VO_2 is a promising method to achieve dynamic tunable characteristics in the THz range. In 2018, Song et al. presented an active absorption device based on VO_2 metamaterials, 90% absorptance bandwidth reaches 0.33 THz with a central frequency of 0.55 THz, and absorptance at peak frequencies can be continuously tuned from 30% to 100% [25]. In order to improve operation bandwidth, in 2019, Bai et al. designed a broadband THz absorber that the bandwidth of absorption rate above 90% is 1.25 THz, and the absorption rate can be continuously tuned from 15% to 96% [26]. To achieve multi-band absorption, in 2020, Huang et al. presented a dual broadband absorber, the bandwidths with the absorption above 80% were 0.88 THz and 0.77 THz in the frequency ranges of 0.56–1.44 THz and 2.88–3.65 THz, and the absorptance can be continuously adjusted from 20% to 90% [27]. Although the performance of absorbers based on vanadium dioxide metamaterials has been improved, the characteristics of the broad bandwidth, multi-band and active control still require more research to meet the expectations of practical applications.

For the classic three-layer structure absorber, the material and the structure of the top layer design are the most critical parts. In this work, we propose a tunable dual broadband THz absorber, which consists of a VO_2 structure with two perpendicularly intersecting ellipses and a circular hole in the center, and a metal ground plane separated by a dielectric spacer. The conductivity of VO_2 can be controlled by changing the temperature, thereby inducing the transition of VO_2 from an insulator to a metal. Under thermal control, the absorptance of the two bands of the absorber can be continuously tuned. The physical mechanism of MPA is investigated by the impedance matching and interference theory. The electric field analysis is discussed to gain a deeper understanding of the absorption mechanism. Moreover, it is verified that the absorptance is independent of polarization through the incidence of different polarization angles. The influence of the geometrical parameters of the structure on the absorber is discussed. This kind of tunable dual broadband perfect absorber has considerable application prospects in the field of THz technology.

2. Materials and Methods

The design structure of the absorber is shown in Figure 1. It consists of a three-layer structure: VO_2 on the top layer, a dielectric layer in the middle layer and a metal substrate on the bottom layer. The period of the structural unit is p = 30 μm. The top layer is composed of VO_2 with a thickness of 0.08 μm. As is shown in Figure 1b, the pattern is composed of two perpendicularly intersecting ellipses and a circular hole in the center. The lengths of the semi-major axis and semi-minor axis of the ellipse and the radius of the inner circle are a = 14 μm, b = 9 μm and c = 6 μm, respectively. The dielectric constant of VO_2 can be expressed by the Drude model [28], which is:

$$\varepsilon(\omega) = \varepsilon_\infty - \frac{\omega_p^2(\sigma)}{(\omega^2 + i\gamma\omega)} \tag{1}$$

where ε_∞ and γ are 12 and 5.75×10^{13} rad/s, respectively. The relationship between plasma frequency and conductivity is:

$$\omega_p^2(\sigma) = \frac{\sigma}{\sigma_0}\omega_p^2(\sigma_0) \tag{2}$$

with $\sigma_0 = 3 \times 10^5$ S/m and $\omega_p(\sigma_0) = 1.4 \times 10^{15}$ rad/s. The middle layer is silicon dioxide (SiO_2) with a thickness of 12 μm and a permittivity (ε) of 3.8 [29]. The bottom layer is composed of gold with a thickness of 0.2 μm and a conductivity of 4.56×10^7 S/m. As shown in Figure 1a, the incident wave propagates along the *Z*-axis from top to bottom, and the electric field polarization direction is along the *X*-axis. The spectral response of the structure is calculated by the finite element method. Periodic boundary conditions are applied in the X and Y directions, and a perfect matching layer is applied in the Z direction. The absorptance can be calculated by calculating the reflection coefficient (S_{11}) and the transmission coefficient (S_{21}). The expression of absorptance is:

$$A(\omega) = 1 - R(\omega) - T(\omega) = 1 - \left|S_{11}(\omega)\right|^2 - \left|S_{21}(\omega)\right|^2 \tag{3}$$

due to the thickness of metal is significantly larger than the skin depth to ensure no transmission, $T(\omega) = 0$. The absorptance here can be expressed as:

$$(\omega) = 1 - R(\omega) = 1 - \left|S_{11}(\omega)\right|^2 \tag{4}$$

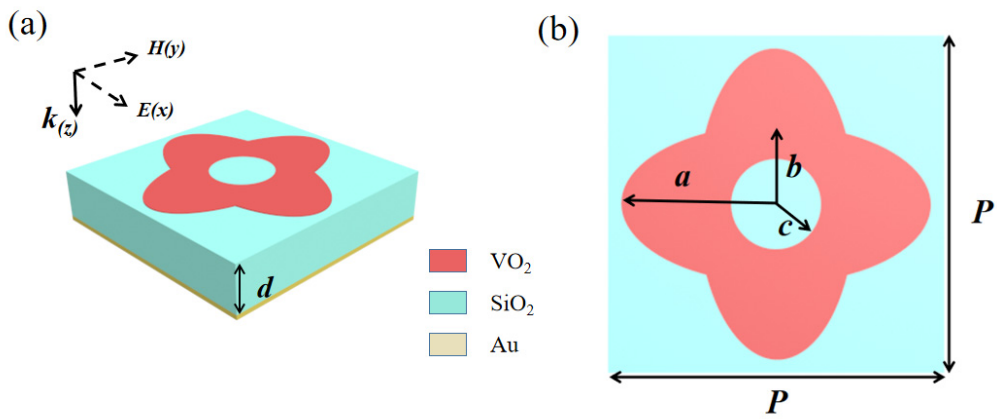

Figure 1. (**a**) Three-dimensional schematic of the absorber. (**b**) Top view of the unit cell.

3. Results

The absorption spectrum and reflection spectrum of the absorber when VO_2 patterns are in the metal phase are shown in Figure 2a. The results show that there are two absorption bandwidths of 90% absorptance reach as wide as 2.32 THz from 1.87 to 4.19 THz and 2.03 THz from 8.70 to 10.73 THz under normal incidence. Moreover, there are also four perfect absorption peaks located at 2.3 THz, 3.6 THz, 8.8 THz and 10.4 THz, respectively. Due to the influence of the polarization angle is one of the most important properties of the absorber, we simulated the absorption spectrum under different polarization angles. Figure 2b is the color map under different polarization angles. Obviously, due to the symmetry of the structure, polarization is insensitive.

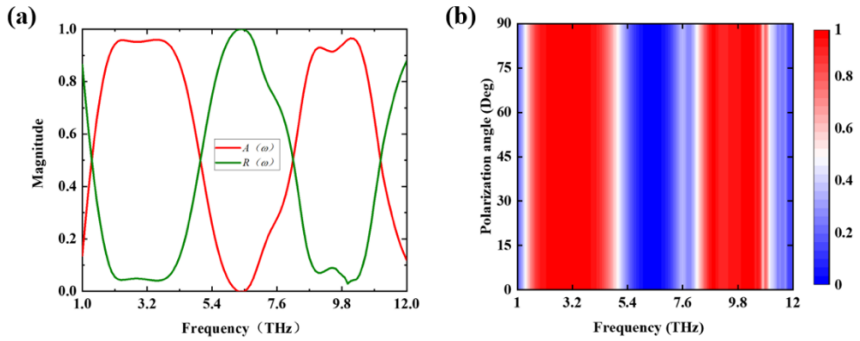

Figure 2. When the conductivity of VO_2 is 2×10^5 S/m. (**a**) The reflection and absorption spectra of the dual broadband absorber. (**b**) Color map of absorption spectra with different polarization angles.

The conductivity of VO_2 can be controlled by adjusting the temperature. The change of conductivity can change the dielectric constant of VO_2. Therefore, the absorptance of the absorber can be continuously tuned by changing the temperature. When the conductivity of VO_2 changes from 200 S/m to 2×10^5 S/m, we can tune the absorption from 2% to 94% at the corresponding frequency range, and the central position of the peak keeps unchanged, as shown in Figure 3. When the conductivity is 2×10^5 S/m, VO_2 appears as a metallic phase, and the best performance of the absorber is achieved. The absorption peaks that appear in the two absorption bands of VO_2 at low conductivity can be explained by wave interference theory. The two absorption peaks in Figure 3b are at 3.21 THz and 9.63 THz, while the corresponding vacuum wavelengths are 93 μm and 31 μm, respectively. The refractive index in the dielectric layer is $\sqrt{\varepsilon}$, and the corresponding wavelengths in the dielectric layer are 48 μm and 16 μm. The thickness of the dielectric layer is d = 12 μm, and the length is precisely the corresponding 1/4 and 3/4 wavelengths, which meets the destructive interference condition between reflection and incidence. When the structural phase of VO_2 is not a metallic phase, the position of the absorption peak is determined by the thickness of the dielectric layer. The presence of VO_2 is to tune the amplitude of absorption peaks. As the conductivity increases, the dielectric constant of VO_2 changes, and the insulating phase gradually approaches the metal phase, and the absorptance gradually increases.

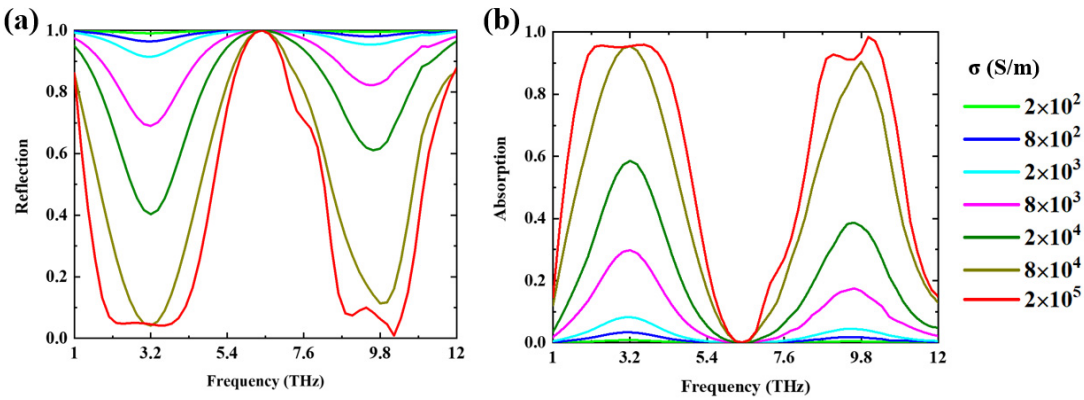

Figure 3. (**a**) Reflection and (**b**) absorption spectra with different conductivity of VO_2.

4. Discussion

Impedance matching theory can be used to explain the phenomenon of perfect absorption. The effective impedance of the MPA can be expressed as [30]:

$$Z_{eff} = \sqrt{\frac{\mu_{eff}}{\varepsilon_{eff}}} = \sqrt{\frac{(1+S_{11})^2 - S_{21}^2}{(1-S_{11})^2 - S_{21}^2}} \tag{5}$$

where μ_{eff} and ε_{eff} are the effective permeability and effective permittivity, respectively. It is well known that impedance matching can be achieved as both of them reach the same. The real and imaginary parts of the impedance are derived from the *S* parameter. As is shown in Figure 4, when the VO_2 conductivity is 2×10^5 S/m, the real parts of the impedance are close to 1, and the imaginary parts of the impedance are close to 0 in the frequency range from 1.87 to 4.19 THz and from 8.70 to 10.73 THz. This means that the impedance of the absorber gradually matches with free space, which is the typical perfect absorber feature [27].

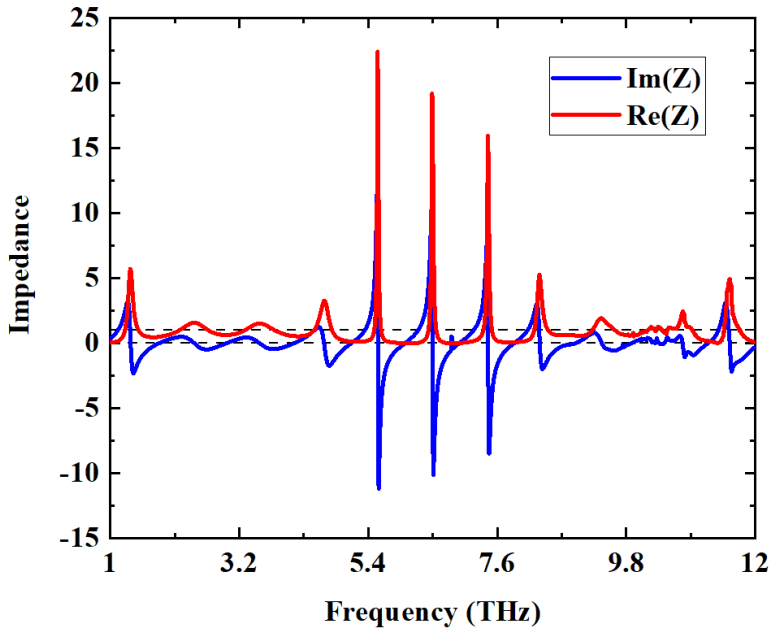

Figure 4. The relative impedance with the conductivities of VO_2 is 2×10^5 S/m.

To further understand the physical mechanism of the absorber, we conducted an electric field analysis. Figure 5 shows the electric field distribution at the four resonance peaks. The first resonance peak is located at 2.3 THz, as shown in Figure 5a; the electric field is mainly concentrated in the gap between the long axis of the ellipse of the two structural units. The second resonance peak is located at 3.6 THz, as shown in Figure 5b; the electric field is mainly concentrated at the long axis of the ellipse and the edge of the inner ring of the unit structure. The combination of the overlapping regions of the two resonance spectra provides a guarantee for high-efficiency broadband absorption [31]. The third resonance peak is located at 8.8 THz, as shown in Figure 5c; the electric field is mainly concentrated in the inner ring and the junction of the two perpendicular ellipses. The fourth resonance peak is located at 10.4 THz, as shown in Figure 5d; the electric field is mainly concentrated at the junction of two ellipses and the gap area of the corresponding unit. Both resonance spectra provide the basis for the second broadband absorption. Due to the symmetry of the structure, similar phenomena also apply when the structure is under the Y-polarized incident wave.

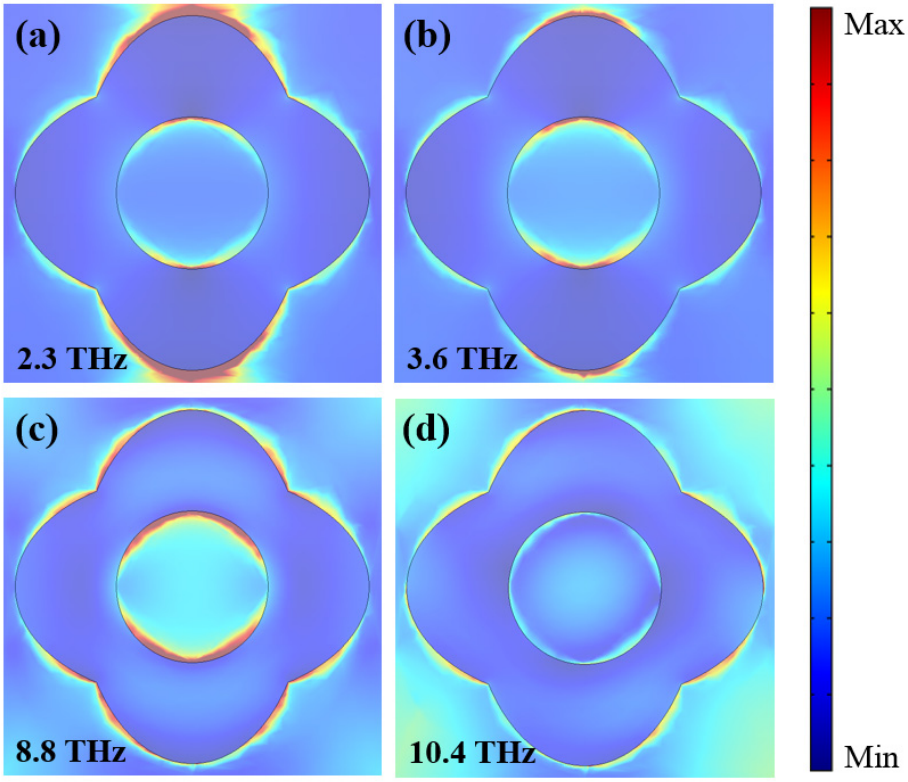

Figure 5. The electric field distribution in the top view at 2.3 THz (**a**), 3.6 THz (**b**), 8.8 THz (**c**) and 10.4 THz (**d**).

To illustrate the importance of geometric structure parameters, it is necessary to verify the influence of geometric structure parameters on the absorber. Figure 6 shows the influence of the major axis of the ellipse *a*, the minor axis of the ellipse *b*, the radius of the inner circle *c* and the thickness of the medium d on the absorptance of the absorber. As shown in Figure 6a, when the major axis of the ellipse becomes longer, the absorption bandwidth becomes wider; however, the absorption efficiency decreases. When the major axis of the ellipse becomes shorter, the absorption bandwidth becomes narrower, but the absorption becomes higher. In Figure 6b, it is obvious that the minor axis of the ellipse has the same changing law. In Figure 6c, conversely, when the radius of the inner circle becomes shorter, the absorption bandwidth becomes wider, and the absorption efficiency decreases. When the radius of the inner circle becomes longer, the absorption bandwidth becomes narrower, and the absorption becomes higher. The position of the resonance peak varies with the change of the major axis and minor axis of the ellipse or the radius of the inner circle. The absorptance and bandwidth will change with the change of the resonance peak position. As shown in Figure 6d, when the thickness of SiO_2 increases, the absorption peak gradually shifts to low frequencies. At the same time, the number of absorption peaks increases and the bandwidth narrows. When the thickness of SiO_2 decreases, the absorption peak gradually shifts to high frequency, and the bandwidth becomes larger. However, the number of absorption peaks and the absorptance decrease. The position of the resonance peak is affected by the thickness of the medium. The position of the resonance peak and the absorptance of the entire absorber are affected by the SiO_2 and VO_2. VO_2 and SiO_2 determine the impedance of the proposed system and have a significant influence on the absorptance and bandwidth. The results further confirmed the important role of geometrical structure parameters in absorber performance. After optimizing the structural parameters, a high-performance tunable dual broadband terahertz absorber is obtained.

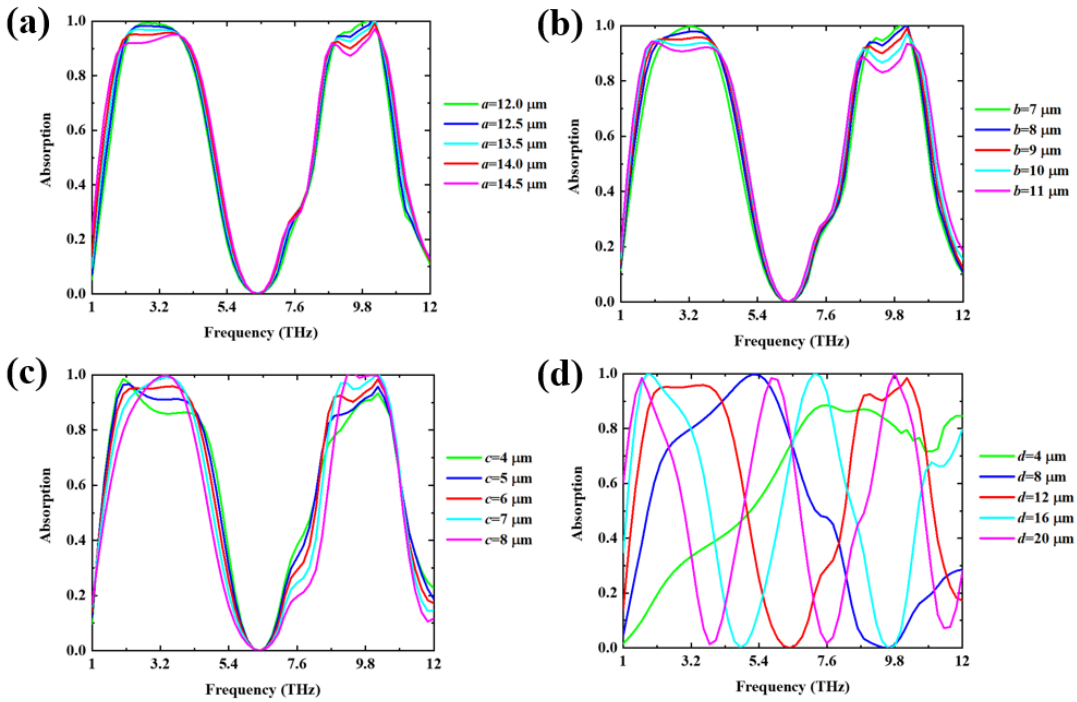

Figure 6. When σ is 2×10^5 S/m, the absorption spectrum changes with the major axis of the ellipse (**a**), the minor axis of the ellipse (**b**), the radius of the inner circle (**c**) and the thickness of SiO_2 (**d**).

5. Conclusions

In conclusion, we propose a tunable dual broadband THz metamaterial absorber. Two VO_2 ellipses that intersect perpendicularly with a circular hole dug out of the center are used as the top structure, the middle layer is SiO_2, and the top layer is gold. Based on interference theory and impedance matching theory, we obtained a tunable absorber with which two bandwidths of 90% absorption reach as wide as 2.32 THz from 1.87 to 4.19 THz and 2.03 THz from 8.70 to 10.73 THz under normal incidence. By changing the conductivity of the VO_2, dynamic absorption control from 2% to 94% can be achieved. Moreover, due to the symmetry of the structure, the absorptance is insensitive to the polarization angle. We envision that our high-performance, tunable, dual broadband absorber may have potential in a vast range of applications in imaging, modulation and stealth technology.

Author Contributions: Conceptualization, X.-F.J.; formal analysis, X.-F.J.; visualization, X.-F.J.; writing, original draft preparation, X.-F.J.; writing, review and editing, X.-F.J., T.L. and Z.-H.Z.; supervision, G.-F.S. and Y.X. All of the authors discussed the results and commented on the manuscript. All authors have read and agreed to the published version of the manuscript.

Funding: This work was supported by National Key Research and Development Plan (No.2016YFB0402402). The Strategic Priority Research Program of the Chinese Academy of Sciences, Grant No. XDB43010000. National Key Research and Development Plan (No.2016YFB0400601). National Basic Research Program of China (973 Program) (No. 2015CB351902). National Science and Technology Major Project (2018ZX01005101-010). National Natural Science Foundation of China (Grant No. 61835011). National Natural Science Foundation of China (Grant No. U1431231). Key Research Projects of the Frontier Science of the Chinese Academy of Sciences (No. QYZDY-SSW-JSC004). Beijing Science and Technology Projects (Grant No. Z151100001615042).

Conflicts of Interest: The authors declare no conflict of interest.

References

1. Koenig, S.; Lopez-Diaz, D.; Antes, J.; Boes, F.; Henneberger, R.; Leuther, A.; Tessmann, A.; Schmogrow, R.; Hillerkuss, D.; Palmer, R.; et al. Wireless sub-THz communication system with high data rate. *Nat. Photonics* **2013**, *7*, 977–981. [CrossRef]
2. Woolard, D.L.; Brown, E.R.; Pepper, M.; Kemp, M. Terahertz frequency sensing and imaging: A time of reckoning future applications? *Proc. IEEE* **2005**, *93*, 1722–1743. [CrossRef]
3. Wu, Q.; Hewitt, T.D.; Zhang, X.C. Two-dimensional electro-optic imaging of THz beams. *Appl. Phys. Lett.* **1996**, *69*, 1026–1028. [CrossRef]
4. Yang, C.; Wang, Z.; Yuan, H.; Li, K.; Zheng, X.; Mu, W.; Yuan, W.; Zhang, Y.; Shen, W. All-Dielectric Metasurface for Highly Tunable, Narrowband Notch Filtering. *IEEE Photonics J.* **2019**, *11*. [CrossRef]
5. Zhang, T.; Zhang, J.; Xu, J.; Wang, Q.; Zhao, R.; Liu, H.; Dong, G.; Hao, Y.; Bi, K. Wideband metasurface filter based on complementary split-ring resonators. *Mod. Phys. Lett. B* **2017**, *31*, 1750222. [CrossRef]
6. Liu, Z.; Guo, L.; Zhang, Q. A Simple and Efficient Method for Designing Broadband Terahertz Absorber Based on Singular Graphene Metasurface. *Nanomaterials* **2019**, *9*, 1351. [CrossRef] [PubMed]
7. Wang, Q.; Zhou, R.; Wang, X.; Guo, Y.; Hao, Y.; Lei, M.; Bi, K. Wideband terahertz absorber based on Mie resonance metasurface. *Aip Adv.* **2017**, *7*, 115310. [CrossRef]
8. Quader, S.; Zhang, J.; Akram, M.R.; Zhu, W. Graphene-Based High-Efficiency Broadband Tunable Linear-to-Circular Polarization Converter for Terahertz Waves. *IEEE J. Sel. Top. Quantum Electron.* **2020**, *26*, 1–8. [CrossRef]
9. Xiao, Z.; Zou, H.; Zheng, X.; Ling, X.; Wang, L. A tunable reflective polarization converter based on hybrid metamaterial. *Opt. Quantum Electron.* **2017**, *49*, 401. [CrossRef]
10. Campbell, S.D.; Grobe, S.D.; Goodin, I.L.; Su, Q.; Grobe, R. Limitations of decomposition-based imaging of longitudinal absorber configurations. *Phys. Rev. A* **2008**, *77*, 023821. [CrossRef]
11. Chen, H.; Ma, W.; Huang, Z.; Zhang, Y.; Huang, Y.; Chen, Y. Graphene-Based Materials toward Microwave and Terahertz Absorbing Stealth Technologies. *Adv. Opt. Mater.* **2019**, *7*, 1801318. [CrossRef]
12. Liu, X.; Fu, G.; Liu, M.; Liu, G.; Liu, Z. High-Quality Plasmon Sensing with Excellent Intensity Contrast by Dual Narrow-Band Light Perfect absorbers. *Plasmonics* **2017**, *12*, 65–68. [CrossRef]
13. Landy, N.I.; Sajuyigbe, S.; Mock, J.J.; Smith, D.R.; Padilla, W.J. Perfect metamaterial absorber. *Phys. Rev. Lett.* **2008**, *100*, 207402. [CrossRef] [PubMed]
14. Bhattacharyya, S.; Ghosh, S.; Srivastava, K.V. Triple band polarization-independent metamaterial absorber with bandwidth enhancement at X-band. *J. Appl. Phys.* **2013**, *114*, 094514. [CrossRef]
15. Cong, L.; Tan, S.; Yahiaoui, R.; Yan, F.; Zhang, W.; Singh, R. Experimental demonstration of ultrasensitive sensing with terahertz metamaterial absorbers: A comparison with the metasurfaces. *Appl. Phys. Lett.* **2015**, *106*, 031107. [CrossRef]
16. Watts, C.M.; Liu, X.; Padilla, W.J. Metamaterial Electromagnetic Wave Absorbers. *Adv. Mater.* **2012**, *24*, OP98–OP120. [CrossRef] [PubMed]
17. Chen, K.; Adato, R.; Altug, H. Dual-Band Perfect Absorber for Multispectral Plasmon-Enhanced Infrared Spectroscopy. *Acs Nano* **2012**, *6*, 7998–8006. [CrossRef]
18. Cao, T.; Wei, C.-W.; Simpson, R.E.; Zhang, L.; Cryan, M.J. Broadband Polarization-Independent Perfect Absorber Using a Phase-Change Metamaterial at Visible Frequencies. *Sci. Rep.* **2014**, *4*, 3955. [CrossRef]
19. Hedayati, M.K.; Zillohu, A.U.; Strunskus, T.; Faupel, F.; Elbahri, M. Plasmonic tunable metamaterial absorber as ultraviolet protection film. *Appl. Phys. Lett.* **2014**, *104*, 041103. [CrossRef]
20. Hedayati, M.K.; Faupel, F.; Elbahri, M. Tunable broadband plasmonic perfect absorber at visible frequency. *Appl. Phys. Mater. Sci. Process.* **2012**, *109*, 769–773. [CrossRef]
21. Andryieuski, A.; Lavrinenko, A.V. Graphene metamaterials based tunable terahertz absorber: Effective surface conductivity approach. *Opt. Express* **2013**, *21*, 9144–9155. [CrossRef]
22. Wang, R.; Li, L.; Liu, J.; Yan, F.; Tian, F.; Tian, H.; Zhang, J.; Sun, W. Triple-band tunable perfect terahertz metamaterial absorber with liquid crystal. *Opt. Express* **2017**, *25*, 32280–32289. [CrossRef]
23. Pu, M.; Wang, M.; Hu, C.; Huang, C.; Zhao, Z.; Wang, Y.; Luo, X. Engineering heavily doped silicon for broadband absorber in the terahertz regime. *Opt. Express* **2012**, *20*, 25513–25519. [CrossRef] [PubMed]
24. Wen, Q.-Y.; Zhang, H.-W.; Yang, Q.-H.; Xie, Y.-S.; Chen, K.; Liu, Y.-L. Terahertz metamaterials with VO_2 cut-wires for thermal tunability. *Appl. Phys. Lett.* **2010**, *97*, 021111. [CrossRef]

25. Song, Z.; Wang, K.; Li, J.; Liu, Q.H. Broadband tunable terahertz absorber based on vanadium dioxide metamaterials. *Opt. Express* **2018**, *26*, 7148–7154. [CrossRef]
26. Bai, J.; Zhang, S.; Fan, F.; Wang, S.; Sun, X.; Miao, Y.; Chang, S. Tunable broadband THz absorber using vanadium dioxide metamaterials. *Opt. Commun.* **2019**, *452*, 292–295. [CrossRef]
27. Huang, J.; Li, J.; Yang, Y.; Li, J.; Ii, J.; Zhang, Y.; Yao, J. Active controllable dual broadband terahertz absorber based on hybrid metamaterials with vanadium dioxide. *Opt. Express* **2020**, *28*, 7018–7027. [CrossRef]
28. Wang, S.; Kang, L.; Werner, D.H. Hybrid Resonators and Highly Tunable Terahertz Metamaterials Enabled by Vanadium Dioxide (VO_2). *Sci. Rep.* **2017**, *7*, 1–8. [CrossRef]
29. Naftaly, M.; Miles, R.E. Terahertz time-domain spectroscopy of silicate glasses and the relationship to material properties. *J. Appl. Phys.* **2007**, *102*, 043517. [CrossRef]
30. Smith, D.R.; Schultz, S.; Markos, P.; Soukoulis, C.M. Determination of effective permittivity and permeability of metamaterials from reflection and transmission coefficients. *Phys. Rev. B* **2002**, *65*, 195104. [CrossRef]
31. Song, Z.; Jiang, M.; Deng, Y.; Chen, A. Wide-angle absorber with tunable intensity and bandwidth realized by a terahertz phase change material. *Opt. Commun.* **2020**, *464*, 125494. [CrossRef]

Publisher's Note: MDPI stays neutral with regard to jurisdictional claims in published maps and institutional affiliations.

© 2020 by the authors. Licensee MDPI, Basel, Switzerland. This article is an open access article distributed under the terms and conditions of the Creative Commons Attribution (CC BY) license (http://creativecommons.org/licenses/by/4.0/).